ACS OMEGA

http://pubs.acs.org/journal/acsodf

Article

$Ni_{12}P_5$/P−N−C Derived from Natural Single-Celled Chlorella for Catalytic Depolymerization of Lignin into Monophenols

Xin Zhao, Yingying Yang, Jingyu Xu, Yanzhu Guo, Jinghui Zhou, and Xing Wang*

Cite This: *ACS Omega* 2022, 7, 13134−13143

Read Online

ACCESS | Metrics & More | Article Recommendations | Supporting Information

ABSTRACT: Lignin is exceptionally abundant in nature and is regarded as a renewable, cheap, and environmentally friendly resource for the manufacture of aromatic chemicals. A novel $Ni_{12}P_5$/P−N−C catalyst for catalytic hydrogenolysis of lignin was synthesized. The catalysts were prepared by simple impregnation and carbonization using the nonprecious metal Ni taken up by the cell wall of Chlorella in $Ni(NO_3)_2$ solution. There were only two steps in this process, making the whole process very simple, efficient, and economical. $Ni_{12}P_5$ was uniformly distributed in the catalyst. During the hydrogenolysis of lignin, after 4 h reaction at 270 °C, the yield of bio-oil reached 65.26%, the yield of monomer reached 9.60%, and the selectivity to alkylphenol reached 76.15%. The mixed solvent of ethanol/isopropanol (1:1, v/v) is used as the solvent for the hydrogenolysis of lignin, which not only had excellent hydrogen transferability but also improved the yield of bio-oil, inhibiting the generation of char. No external hydrogen was used, thus avoiding safety issues in hydrogen transport and storage.

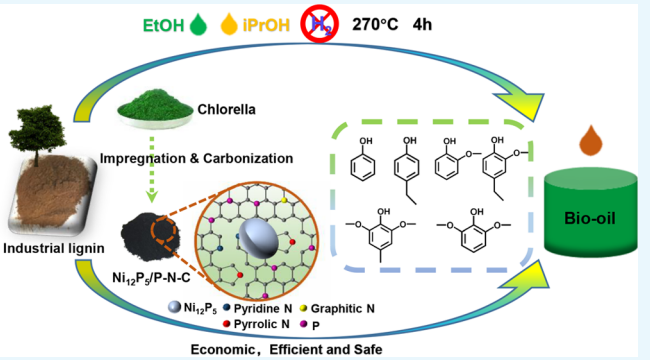

1. INTRODUCTION

The depletion of fossil fuels and the massive demand for energy and social production has led to a great deal of intensive research into sustainable fuel and chemical production.[1,2] Lignocellulosic biomass, as a natural renewable resource containing benzene rings, has received increasing attention for its potential application as an alternative to petroleum-based fuels and chemicals.[3] Lignin is a highly complex natural lignocellulose polymer, composed of various lignin precursors, such as coniferol, p-coumarol, and myrosinol,[1] through multiple linkages such as β-O-4, α-O-4, β-5,[4] etc., which are connected into a three-dimensional network space structure. Lignin has the advantages of a wide range of sources and low cost.[5] The global pulp and paper industry produces about 50 million tons of lignin every year. At present, most of this lignin is directly incinerated for heating or power generation.[6] Catalytic depolymerization of lignin into phenolic monomers is a vital way to utilize lignin efficiently. However, due to the different complex structures brought by the extraction method and the biomass types of lignin, effective depolymerization of lignin to obtain abundant high-value platform compounds remains a challenging problem.[7]

Diversiform chemical conversion processes, including catalytic hydrogenolysis,[7] pyrolysis,[8] photocatalysis,[9] and catalytic oxidation,[10] have been studied for the sake of an efficient method to convert lignin into high value-added chemicals. Among them, the catalytic hydrogenolysis of lignin is a very effective method for depolymerization of lignin, which can significantly reduce the content of char produced during the lignin depolymerization process, and the conversion rate and selectivity of the monomers are desirable.[11] Alcohol-based solvents, such as methanol, ethanol, and isopropanol, are often used as solvent systems for the hydrogenolysis of lignin, due to its in situ hydrogen supply capacity for the hydrogenolysis reaction as well as dissolution of lignin and depolymerization products. However, the hydrogenolysis of lignin in a single solvent system often has limitations that the raw materials and products cannot be well dispersed or the hydrogen supply capacity is poor. Therefore, people turned their attention to the research on the hydrogenolysis of lignin in mixed solvents and found that mixed solvents can overcome many problems in the process of lignin hydrogenolysis caused by a single solvent.[12] Oregui-Bengoechea et al. found that the hydrogenolysis bio-oil yield of rice straw lignin reached 75.80% with ethanol as the reagent and formic acid as the aid. This is because ethanol could stabilize the depolymerization monomer well, while formic acid acts as an efficient in situ hydrogen donor reagent.[13,14]

As a catalyst support, carbon can be chemically functionalized by metallic nanoparticles to obtain or improve catalytic

Received: January 27, 2022
Accepted: March 25, 2022
Published: April 5, 2022

activity.[15] Compared with metal oxide catalyst supports (TiO_2, γ-Al_2O_3, mesoporous silica, etc.), the catalytic performance of carbon-based catalysts can remain excellent after multiple uses, and the structural integrity is more stable in the reaction system of high temperature or pressure. Metal oxide catalysts are more prone to structural collapse and metal precipitation under the same severe reaction conditions, which contaminate the products and also lead to the unrecyclable catalysts.[16] The carbon support of the catalyst can be obtained from biomass and therefore has a wide range of sources and low cost, which have aroused the interest of many researchers. However, excellent specific surface area and porosity carbon materials prepared from biomass usually require some complicated and expensive processing procedures, including carbonization, activation, impregnation, reduction, and other steps, and also require a lot of expensive and dangerous reagents and chemicals.[17−20] Therefore, it is very reasonable to design an inexpensive and simple method to prepare carbon-based metal catalysts from biomass feedstocks.

Herein, natural single-celled Chlorella was used as a carbon source, and through the ability of the Chlorella cell wall to passively adsorb metal ions in solution, Ni^{2+} ions in solution were taken up by simple direct impregnation and stirring, and a novel catalyst containing Ni phosphide was obtained by direct carbonization in N_2. X-ray diffraction (XRD) and X-ray photoelectron spectroscopy (XPS) patterns confirmed that Ni in the catalyst exists in the form of $Ni_{12}P_5$. Transmission electron microscopy (TEM) and scanning electron microscope−energy-dispersive spectroscopy (SEM−EDS) analyses showed that the $Ni_{12}P_5$ nanoparticles supported by this novel catalyst had large loading and uniform distribution. The catalyst was used for catalytic hydrogenolysis of lignin, a byproduct produced in industrial production. An ethanol/isopropanol (1:1, v/v) mixed solvent was selected as the solvent system for the reaction, and the obtained bio-oil and phenolic monomers were much higher than the single solvent system without adding external hydrogen. 2D HSQC NMR and gel permeation chromatography (GPC) data revealed the breakage of major lignin linkages and formation of low molecular weight polymers or monomers. Analysis of the monomers in the bio-oil by the gas chromatography−mass spectrometer (GC−MS) and gas chromatography−flame ionization detector (GC−FID) indicated that the monomers were mainly present as alkylated phenolic products.

2. EXPERIMENTAL SECTION

2.1. Materials and Chemicals. Chlorella was supplied by the Institute of Hydrobiology (Wuhan, China). Lignin was supplied by Longlive Bio-technology Co., Ltd., Shandong, China. Ethanol (EtOH) (AR, 98%), isopropyl alcohol (iPrOH) (AR, 98%), and $Ni(NO_3)_2{\cdot}6H_2O$ (AR, 98%) were purchased from Energy Chemical (Shanghai, China).

2.2. Preparation of $Ni_{12}P_5$/P−N−C Catalysts. Three $Ni_{12}P_5$/P−N−C catalysts with different Ni loadings were prepared by directly immersing Chlorella powder in different concentrations of $Ni(NO_3)_2$ aqueous solution to take up Ni ions, followed by further carbonization treatment. To a clean conical flask, 1, 8, and 15 g of $Ni(NO_3)_2{\cdot}H_2O$ were dissolved in 100 mL of deionized water, then 5 g of Chlorella powder was added, and the mixture was stirred at room temperature for 24 h. After this, the solid part was collected by centrifugation and freeze-dried for 72 h to obtain Ni-adsorbed Chlorella. The Ni-adsorbed Chlorella powder was ground and dispersed uniformly and then placed in a tube furnace for further carbonization. The carbonization conditions were as followed: under an N_2 (20 mL/min) atmosphere, the temperature was raised from room temperature to 800 °C at a heating rate of 2 °C per minute, kept for 2 h, and then dropped to 25 °C in 8 h. For comparison, the Chlorella powder was directly carbonized in an N_2 atmosphere at 800 °C and named as DC. The obtained catalyst and DC were collected and stored in a desiccator. Three catalysts with different $Ni_{12}P_5$ loading contents were named as $Ni_{12}P_5$/P−N−C−x, where x represents the different concentrations (wt %) of $Ni(NO_3)_2$ aqueous solution during impregnation. With the concentrations of 1, 8, and 15%, the relative "x" was 1, 2, and 3, respectively.

2.3. Catalytic Test and Instrumental Analysis Methodology. The hydrogenolysis of lignin was performed in a 50 mL autoclave with a magnetic stirring and heating system. Lignin (0.2 g) and a certain amount of catalyst were directly added to the autoclave. After adding magnetron and 20 mL of solvent, the autoclave was completely closed and the reaction was carried out at presupposed temperature. After the reaction reaches the end, the heating button was turned off immediately, the autoclave was taken out, and it was put into ice water to quench the further progress of the reaction. The obtained solid−liquid mixture was filtered using 0.22 μm nylon membrane filter to separate the solid and liquid phases. Then, 0.5 mL of n-tetradecane (1.905 mg/mL) was added into the liquid-phase product as an internal standard, and 1 mL was taken for further GC−MS and GC−FID analyses. The solid-phase product was washed three times with 60 mL of ethanol and dried in a vacuum drying oven for 24 h to obtain the used catalyst and char. Bio-oil was obtained through rotary evaporation of the washed liquid for 30 min. All experiments were reproduced in triplicate.

GPC (Waters Co., USA) was employed to determine the molecular weight of the bio-oil sample. The sample (10 mg) was dissolved in 2.5 mL of HPLC-grade tetrahydrofuran (Macklin Co., Ltd., Shanghai, China) and analyzed at 35 °C.

2D HSQC NMR spectra of feedstock lignin and bio-oil were obtained using a Bruker AVIII 400 MHz spectrometer, and the program was applied according to a previous report.[21] In short, 80 mg of sample was dissolved in 0.6 mL of DMSO-d_6, which was also the internal reference.

GC−MS (Agilent 7890A) was employed for the detailed identification of monomers in liquid fraction products. The oven temperature was held at 50 °C for 3 min, then ramped to 275 at 6 °C/min, and held for 5 min after reaching 275 °C. The delay of solvent access into the MS detector was set as 6 min.

GC (Agilent 8890) equipped with a flame ionization detector (GC−FID) was employed for quantitative analysis of the monomer in liquid fraction products. The working program of GC is as follows: FID: 250 °C; carrier gas, N_2; the oven temperature program was the same as GC−MS. The quantification of the monomer in bio-oil employed an effective carbon number method[22] to calculate the relative response factor of the compound, and n-tetradecane was used as the internal standard. Results are the average of three experiments. The yields of bio-oil, monomers, and char and the selectivity of alkylphenol calculation are as follows:

$$\text{Yield of bio} - \text{oil (wt\%)} = (W_{\text{b}-1-\text{o}}/W_{\text{L}}) \times 100\% \quad (1)$$

https://doi.org/10.1021/acsomega.2c00564
ACS Omega 2022, 7, 13134−13143

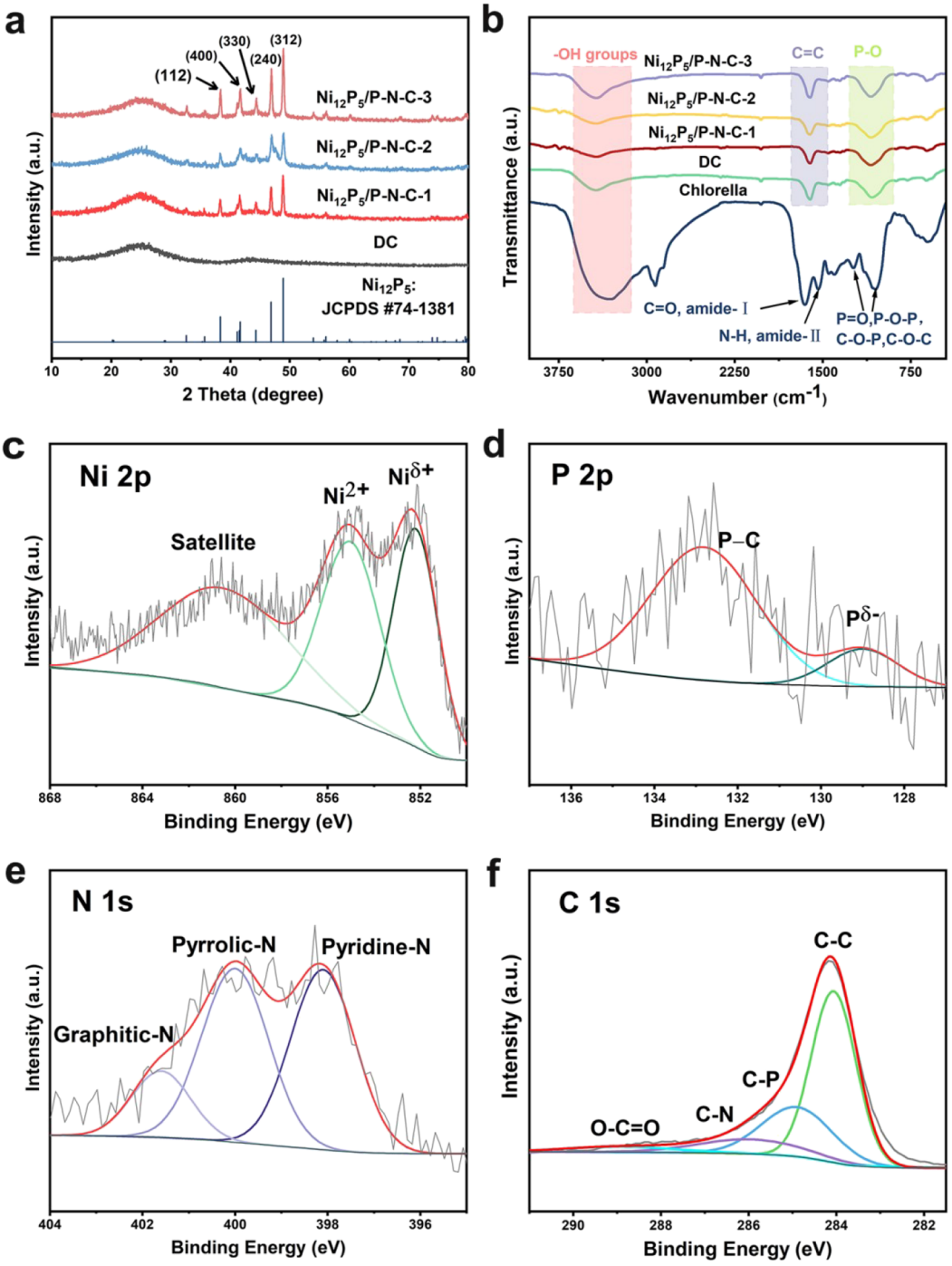

Figure 1. (a) XRD patterns and (b) FT-IR spectra of $Ni_{12}P_5$/P−N−C−1, $Ni_{12}P_5$/P−N−C−2, $Ni_{12}P_5$/P−N−C−3, DC, and Chlorella. (c) Ni 2p, (d) P 2p, (e) N 1s, and (f) C 1s XPS spectra of $Ni_{12}P_5$/P−N−C−2.

$$\text{Yield of monomers (wt\%)} = (W_{mo}/W_L) \times 100\% \quad (2)$$

$$\text{Yield of char (wt\%)} = (W_{ch}/W_L) \times 100\% \quad (3)$$

$$\text{Selectivity of alkylphenol (wt\%)} = (W_{ap}/W_{mo}) \times 100\% \quad (4)$$

where $W_{b\text{-}o}$, W_{mo}, W_{ch}, W_{ap}, and W_L correspond to the weights of bio-oil, monomers, char, alkylphenol, and feedstock lignin, respectively. (The weights of the monomer and alkylphenol were both calculated by GC−FID.)

2.4. Catalyst Characterization. The XRD patterns of fresh $Ni_{12}P_5$/P−N−C catalysts and DC were recorded using a Shimadzu XRD-6100 X-ray diffraction instrument with Cu Kα radiation from 10° to 80° (5°/min). The XPS spectra of the $Ni_{12}P_5$/P−N−C−2 catalyst were recorded on a Thermo ESCALAB 250XI spectrometer. The morphology and composition of $Ni_{12}P_5$/P−N−C catalysts and Chlorella were recorded by SEM−EDS (Hitachi S-800). TEM analysis of $Ni_{12}P_5$/P−N−C catalysts was observed using a JEOL JEM 2010 microscope. The FT-IR spectrum of $Ni_{12}P_5$/P−N−C and DC was recorded on a PerkinElmer Frontier spectrometer. The pH value of the $Ni(NO_3)_2$ aqueous solution was determined with a Sartorius PB-10 pH meter. Inductively coupled plasma emission spectroscopy (ICP-AES) was

https://doi.org/10.1021/acsomega.2c00564
ACS Omega 2022, 7, 13134−13143

performed using a Perkin-Elmer TJA RADIAL IRIS 1000. The BET surface areas of the catalysts were determined using a Tristar II 3020, USA.

3. RESULTS AND DISCUSSION

3.1. Characterization of $Ni_{12}P_5$/P−N−C Catalysts. A novel $Ni_{12}P_5$/P−N−C catalyst supported by the Chlorella cell wall through direct impregnation and carbonization was synthesized. The XRD patterns of three $Ni_{12}P_5$/P−N−C catalysts are shown in Figure 1a. The XRD curves of DC only exhibited a broad peak between 16° and 32°, attributed to the formation of amorphous carbon after carbonization. In control of DC, there were a series of additional peaks in diffraction patterns of $Ni_{12}P_5$/P−N−C catalysts. They were major lattice planes of $Ni_{12}P_5$: (112), (400), (330), (240), and (312) (JCPDS PDF#74-1381).[23] It is observed that there did not exist an obvious difference in the main kinds of $Ni_{12}P_5$ peaks between three $Ni_{12}P_5$/P−N−C catalysts. However, in the pattern of $Ni_{12}P_5$/P−N−C−1, the peaks were clearly sharp, as well as in the pattern of $Ni_{12}P_5$/P−N−C−3. These results can be interpreted as a smaller particle size of $Ni_{12}P_5$ dispersed in the $Ni_{12}P_5$/P−N−C−2 catalyst. The XPS spectra of $Ni_{12}P_5$/P−N−C−2 are shown in Figure 1. As shown in Ni 2p spectra, three peaks located at binding energies of 852.62, 856.51, and 860.52 eV were assigned to the $Ni^{\delta+}$ ($0 < \delta < 2$) species in Ni phosphide,[24] Ni^{2+} in NiO,[25] and satellite signal. The existence of NiO may be due to the formation of superficial oxide layers on the catalyst.[26] The $Ni^{\delta+}$ species in $Ni_{12}P_5$/P−N−C catalysts possessed slightly positive charge acting as a crucial active site during the lignin hydrogenolysis process. As shown in Figure 1d, the peaks at 129.51 eV were assigned to $P^{\delta-}$ ($0 < \delta < 1$), which was an active site for lignin hydrogenolysis. The peaks at 133.13 eV were attributed to the existence of the carbon phosphorus bond. The $P^{\delta-}$ species with a small negative charge also played the role of catalytic active sites in the lignin depolymerization process. Similarly, as shown in Figure 1e, the N 1s spectra of the catalyst revealed graphitic N, pyrrolic N, and pyridinic N species at 401.91, 400.56, and 398.63 eV, respectively. Pyridinic N and pyrrolic N can transfer one p-electron to the aromatic π-system and can effectively change the charge delocalization of the C atom;[27] thus, it can play the role of the active site for lignin catalytic hydrogenolysis in the $Ni_{12}P_5$/P−N−C catalyst. The C 1s spectra of $Ni_{12}P_5$/P−N−C−2 as shown in Figure 1f clearly exhibited four peaks related to O−C═O (288.45 eV), C−N (285.90 eV), C−P (284.87 eV), and C−C (284.15 eV), indicating the existence of the carbon skeleton, phosphide, nitride, and oxidation species in the catalyst. The XPS spectra of $Ni_{12}P_5$/P−N−C−2 proved that the Ni element existed in the form of Ni phosphide in the catalyst doped with nitrogen supported by carbon. The catalytic active site $Ni^{\delta+}$, $P^{\delta-}$, pyridinic N, and pyrrolic N synergistically catalyzed the lignin hydrogenolysis process.

The SEM and TEM images of Chlorella and three $Ni_{12}P_5$/P−N−C catalysts are shown in Figure 2. It was observed that the morphology of all catalysts was lumps of different sizes with uneven surfaces as shown in Figure 2b−d. Chlorella cells of different sizes had walls of different thicknesses, which might result in the various sizes of Ni-supported broken Chlorella cell walls. The folds on the surface of the catalyst were corresponding to the uneven surface of the Chlorella cell wall, which was also of benefit to increase the specific surface area and catalytic activity of the $Ni_{12}P_5$/P−N−C catalyst. The N_2 adsorption isotherms of DC, $Ni_{12}P_5$/P−N−C−1, $Ni_{12}P_5$/P−N−C−2, and $Ni_{12}P_5$/P−N−C−3 (Figure S2 and Table S2) indicated the existence of mesopores in catalysts. The distribution and particle size of supported $Ni_{12}P_5$ in the catalyst can be observed by TEM analysis. As we can see in Figure 2g, the $Ni_{12}P_5$ particles in the $Ni_{12}P_5$/P−N−C−2 catalyst were well-dispersed with different particle sizes. The high-magnification HR-TEM images of $Ni_{12}P_5$/P−N−C−2 are shown in Figure S1 and indicate that the interplanar crystal spacing values of 0.181 nm were assigned to $Ni_{12}P_5$ (312). The existence of $Ni_{12}P_5$ particles in the catalyst was proved. The EDS mapping of $Ni_{12}P_5$/P−N−C−2, as shown in Figure 2e, also proved the good distribution of both Ni and P elements. A minority of $Ni_{12}P_5$ particles were agglomerated as shown in the TEM image, which might have resulted from the high carbonization temperature.[3] The TEM images of $Ni_{12}P_5$/P−N−C−1 (Figure 2f) and $Ni_{12}P_5$/P−N−C−3 (Figure 2h) clearly indicated that a few of the $Ni_{12}P_5$ particles were supported on the catalyst, and indicated the excessive size and the agglomeration of $Ni_{12}P_5$ particles. These results were in accord with the crystal particles displayed in XRD data. Table S1 indicates the content of Ni and P elements on the catalyst by weight (wt %). As we can see, the $Ni_{12}P_5$/P−N−C−2 loaded the highest content of Ni up to 12.83 wt % in comparison with the other two catalysts. This phenomenon indicated that the adsorption effect of the Chlorella cell wall on Ni ions in the solution is related to the concentration of $Ni(NO_3)_2$ solution. Under the same conditions, with an increase in the concentration of $Ni(NO_3)_2$ solution, the absorbed Ni in the cell wall showed an increasing trend at first and then a decreasing trend. The ICP-AES data of the amount of Ni ions absorbed by the chlorella cell wall were also consistent with these results (Table S3). The pH value of $Ni(NO_3)_2$ solution with different concentrations was recorded as shown in Figure S3, indicating that too low pH inhibited the absorption of Ni ions in solution by the chlorella cell wall.

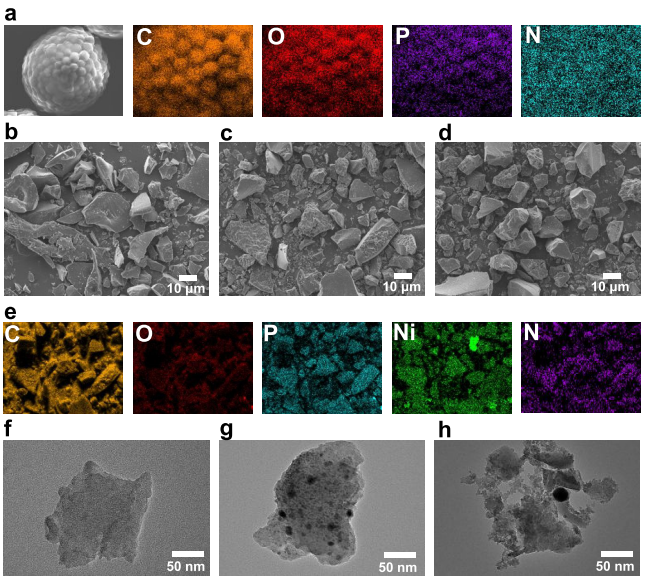

Figure 2. Morphology and structure of the Chlorella and $Ni_{12}P_5$/P−N−C catalysts. (a) SEM images and SEM−EDS elemental mapping results of Chlorella. SEM images of (b) $Ni_{12}P_5$/P−N−C−1, (c) $Ni_{12}P_5$/P−N−C−2, and (d) $Ni_{12}P_5$/P−N−C−3. (e) SEM−EDS elemental mapping results of $Ni_{12}P_5$/P−N−C−2. TEM images of (f) $Ni_{12}P_5$/P−N−C−1, (g) $Ni_{12}P_5$/P−N−C−2, and (h) $Ni_{12}P_5$/P−N−C−3.

https://doi.org/10.1021/acsomega.2c00564
ACS Omega 2022, 7, 13134−13143

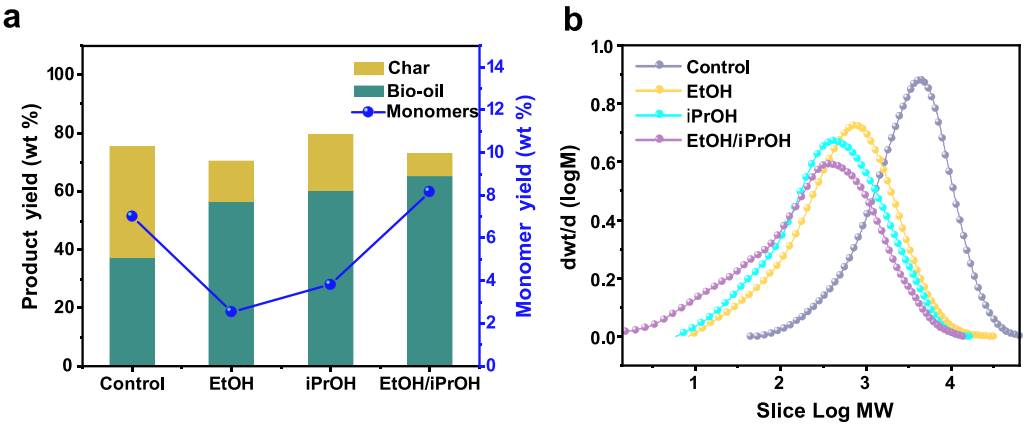

Figure 3. (a) Comparison of product yield and (b) molecular weight distribution of lignin and bio-oil products of different solvents. Reaction conditions: 0.2 g of lignin; 0.2 g of $Ni_{12}P_5$/P−N−C−2 catalyst (0.2 g), 20 mL of EtOH, iPrOH, or EtOH/iPrOH (1:1, v/v), respectively; 270 °C, and 4 h. The control group has as the same conditions of other groups except without addition of the catalyst.

Based on the above results, the $Ni_{12}P_5$/P−N−C−2 catalyst supports a large amount of Ni with good distribution and uniform size, which is considered to have good catalytic activity.

The preparation of the catalysts that used biomass or activated carbon-supported transition metals had been reported previously.[3,28] Transition metal cations, such as Ni ions, were adsorbed by supports in solution and formed as Ni/C catalysts through a process of carbonization and reduction. However, the carbonization process of Ni-supported cell walls of Chlorella in our work did not reduce the Ni element into Ni metal, but the formation of Ni phosphide was undoubtedly proved through XRD patterns and EDS mapping of catalysts. Thus, it is necessary to investigate the mechanism of the formation of $Ni_{12}P_5$/P−N−C catalysts.

The solid cell wall of Chlorella is mainly composed of proteins, lipids, cellulose, hemicellulose, amino-polysaccharides, etc.[29] The surface of the thin-walled spherical structure of this complex composition is scattered with active groups everywhere[30] that can bind metal ions, such as hydroxyl, carboxyl, amino, and various oxygen-containing functional groups. The mechanism of the Ni ion uptake process was mainly attributed to the passive uptake by charged polysaccharides on the cytoderm of Chlorella.[31,32] Figure 1b exhibits the FTIR spectrum of Chlorella powder. The peak at around 3340 cm^{-1} was assigned to the OH group. The strong absorption band in the range of 3000 to 2800 cm^{-1} was assigned to stretching of $>CH_2$, CH, and $-CH_3$ groups. The peaks in the regions of 1700−1600 and 1600−1500 cm^{-1} were ascribed to amide-I and amide-II, respectively, attributed to the existence of the N−H bond.[33] The stretching of the P═O double bond in the phospholipids of the Chlorella cell wall and the vibration of the P−O bond in the polysaccharides appeared in the region between 1250 and 900 cm^{-1}, as shown in the FTIR spectra,[34] which possibly related to the formation of Ni phosphide in catalysts. Besides, the superposed bands between 1200 and 900 cm^{-1} are also ascribed to C−O−P stretching of polysaccharides.[34] Because the absorption of various polysaccharides in the cell wall was complex, definite assignments were unreasonable. EDS mapping of the Chlorella powder sample as shown in Figure 2a clearly exhibited the abundant and uniformly distributed C, O, P, and N elements, which belonged to the metal-absorption functional groups on the Chlorella cell wall. After carbonization, most stretching of functional groups in the FTIR spectra was obviously decreased in intensity or disappeared. Additional C═C stretching to alkenes was assigned at 1620 cm^{-1}. These results possibly explained the reason why Ni phosphide formed during the carbonization process, that is to say, oxygen-containing groups, amides, or phospholipids combined with Ni^{2+} through coordinate or electrostatic approaches proceeded a series of complex redox reactions at high temperatures, and $Ni_{12}P_5$ crystals were mainly formed.

3.2. Effect of Hydrogen Supply Reagents on $Ni_{12}P_5$/P−N−C Catalyst Activity. For lignin hydrodepolymerization processes, the hydrogen source is generally divided into two types: hydrogen and hydrogen supply reagents, with organic solvent hydrogen supply reagents being relatively safe compared to hydrogen. Cheng et al.[35] hold the view that mixed solvents exhibited synergistic capability and acted as a catalyst for hydrogenolysis depolymerization of lignin with a good monomer yield. Herein, an EtOH/iPrOH (1:1, v/v) mixed solvent was employed as the solvent reaction system for $Ni_{12}P_5$/P−N−C-catalyzed depolymerization of lignin. As shown in Figure 3a, in comparison with the lignin hydrogenolysis process in the EtOH system, the reaction conducted in iPrOH achieved a higher monomer yield (3.82 wt %) and more bio-oil (60.34 wt %). These results were in line with the views of Kim et al.[36] that two alkyl groups led to a higher electron-releasing inductive effect meant to better the H-donor ability of iPrOH compared with EtOH, which made iPrOH provide more hydrogen source, resulting in the increase of the yield of low molecular weight lignin and lignin monomers. However, more char was formed during lignin conversion in the iPrOH system (19.32 wt %) compared with the EtOH system (13.89 wt %). It is now understood that EtOH can efficiently prevent the formation of a new C−C bond between lignin fragments and reactive phenolic intermediates through O-alkylation of the phenolic hydroxyl group and C-alkylation of the aromatic ring,[37] which might be the reason for lower amounts of char formed in the EtOH solvent system. In contrast, using pure EtOH and iPrOH systems, reactions conducted in the EtOH/iPrOH system achieved the highest monomer yield (9.60%) and the lowest char (7.63%) amount as shown in Figure 3a. The most likely causes of the results were the good solubility of ethanol for lignin, which reduced the formation of char during lignin conversion, and the good H-donor ability of isopropanol to nucleophilically attacked *β*-

https://doi.org/10.1021/acsomega.2c00564
ACS Omega 2022, 7, 13134−13143

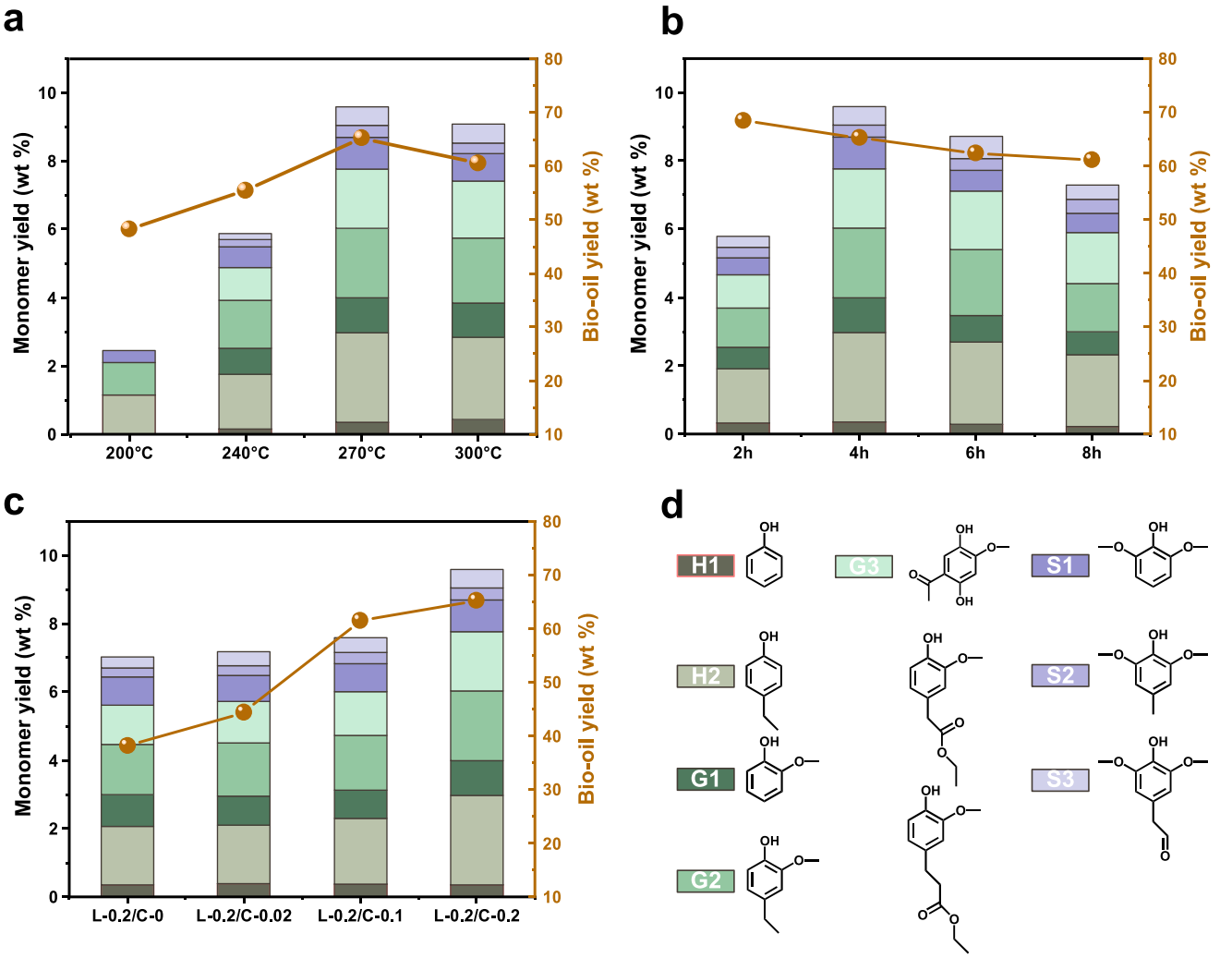

Figure 4. Parameter effects. (a) Reaction temperature effect, conditions: lignin (0.2 g), $Ni_{12}P_5$/P−N−C−2 (0.2 g), EtOH/iPrOH (1:1, v/v) (20 mL), 4 h; (b) reaction time effect, at 270 °C, lignin (0.2 g), $Ni_{12}P_5$/P−N−C−2 (0.2 g), EtOH/iPrOH (1:1, v/v) (20 mL); (c) catalyst dosage effect, at 270 °C, EtOH/iPrOH (1:1, v/v) (20 mL), 4 h; and (d) corresponding structural distributions of main products.

O-4 ether bond-catalyzed depolymerization of lignin.[38] In comparison, the hydrogenolysis of lignin without addition of the $Ni_{12}P_5$/P−N−C−2 catalyst was also conducted in the EtOH/iPrOH system. As shown in Figure 3a, in noncatalytic runs, the yield of bio-oil was relatively lower and the amount of char was comparatively higher than catalytic runs. Recent research[39] had revealed that the hydrogen transfer capacity of EtOH/iPrOH significantly increased by Ni-based catalysts, which was consistent with the promotion of bio-oil and monomer yield as well as the decreased char amount after the addition of the $Ni_{12}P_5$/P−N−C−2 catalyst in the EtOH/iPrOH system. The Guerbet-type reaction was known to inhibit lignin repolymerization through coupling the alcohol products generated during the conversion of lignin to form a new alcohol.[40] The decreased char formation might be because the contribution of Guerbet-type reactions was enhanced in reaction with the addition of the $Ni_{12}P_5$/P−N−C−2 catalyst.

The GPC analysis of large molecular weight phenolics in bio-oil was performed to investigate the difference of the hydrogenolysis effect between EtOH, iPrOH, and EtOH/iPrOH systems. The Mw of feedstock lignin (5178 g/mol), which set as control, was significantly decreased after the lignin conversion process in all three solvents, which was exhibited by the shift of curves toward left, indicating the occurrence of the lignin fragmentation process as shown in Figure 3b. Especially the decrease of bio-oil's Mw (606 g/mol) in the EtOH/iPrOH system was lower than that in both EtOH (1138 g/mol) and iPrOH (868 g/mol) systems, which indicates the increase of the depolymerization degree of bio-oil obtained from EtOH/iPrOH. Thus, the self-supplying hydrogen mixed solvent system of EtOH/iPrOH exhibited excellent intermolecular hydrogen transferability, enhanced bio-oil and monomer yields, and inhibited char formation, which was used for the following series of catalyst activity tests.

3.3. Monophenol Distribution during $Ni_{12}P_5$/P−N−C-Catalyzed Depolymerization of Lignin. To further understood the influence of the $Ni_{12}P_5$/P−N−C catalyst in lignin monomer yield improvement, the identification and quantification of bio-oil were performed by GC−MS and GC−FID, respectively, and the detailed structure of the obtained monomers is shown in Figure 4. The effect of the reaction temperature on the hydrogenolysis of lignin catalyzed by the $Ni_{12}P_5$/P−N−C catalyst was investigated, and the results are shown in Figure 4a. The yield of bio-oil was 48.21 wt % at 200 °C, reached 65.26 wt % at 270 °C, and decreased to 60.47 wt % at 300 °C. The monomer yield exhibited the same tendency

https://doi.org/10.1021/acsomega.2c00564
ACS Omega 2022, 7, 13134−13143

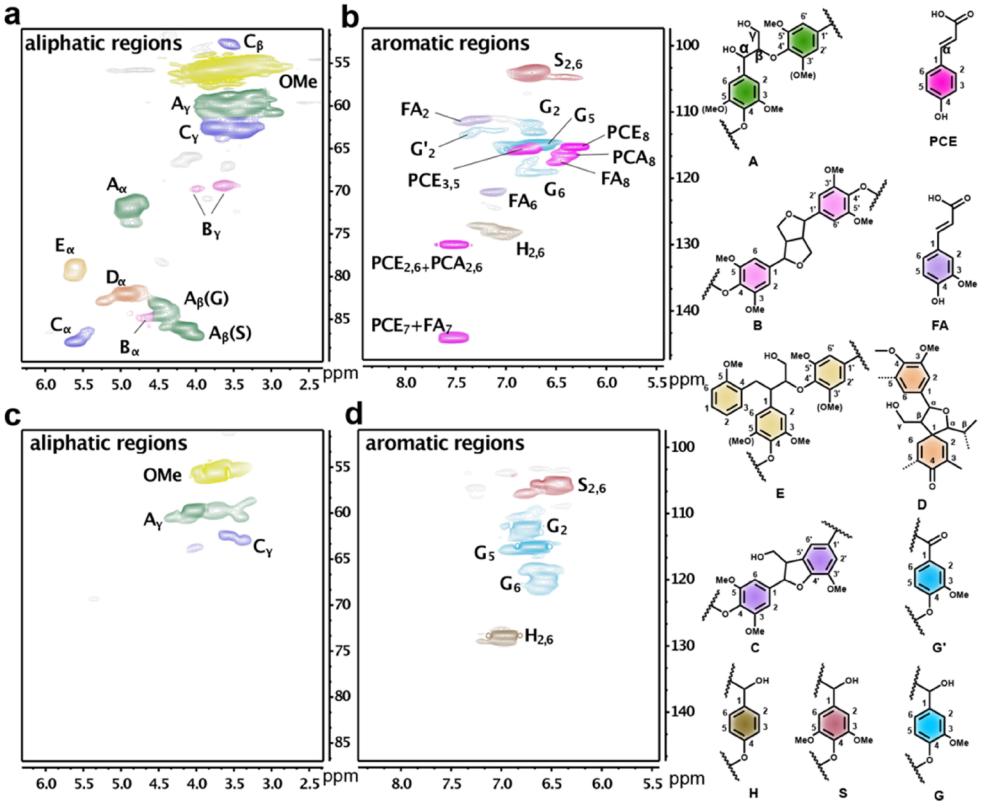

Figure 5. 2D HSQC NMR spectra of feedstock lignin and bio-oil and the main structures: (A) β-O-4′ linkages; (B) resinols; (C) phenylcoumarans; (D) spirodienones; (E) α, β-diaryl ethers; (p-CE) p-coumarates; (p-FA) ferulates; (H) *p*-hydroxyphenyl units; (G) guaiacyl units; (G′) oxidized syringyl units bearing a carbonyl group at Cα; and (S) syringyl units

as bio-oil of first increasing and then decreasing. The maximum value of monomer yield was also at 270 °C. This phenomenon demonstrated that the increase in temperature is accompanied by the improvement in the degree of lignin hydrogenolysis. However, the inhibition of lignin hydrogenolysis had occurred, as the reaction temperature was further increased. The decrease in the yield of lignin hydrogenolysis products might be ascribed to the occurrence of repolymerization and condensation reaction between low molecular weight monomers at high temperatures.[41] The results determined by GC-MS and the corresponding distribution of main monomer products are listed in Figure 4 in detail. Most of the monomer products were H, G, and S-type alkylphenol products because the $Ni^{\delta+}$ active site of $Ni_{12}P_5$/P−N−C−2 can directly hydrogenate the lignin benzene ring or side chain to generate alkyl products in the hydrogen-donating system.[25] Through careful calculation, the selectivity of alkylphenol gradually decreased from 200 to 300 °C (from almost 100% at 200 °C to 75.47% at 300 °C), and the esterified phenolic monomer increased, which might be because the condensation reaction became more intense with the increase of temperature. High-temperature-induced char formation also adhered to the catalyst surface, deactivated the Ni sites, and reduced the selectivity of the alkylation reaction. In addition, G3 products were identified as two different phenyl esters. The possible potential path for the formation of G3 is as follows: O_2 contained in the unexhausted air in the reactor oxidized the β or γ position of lignin to carboxyl groups, and then, the side chain undergoes an esterification reaction with ethanol in the solvent. The content of G3 products increased with the rise of temperature, which actually resulted in the decreased yield of alkylated phenolic products. Thus, the temperature had a significant impact on product distribution and selectivity, as well as monomer and bio-oil yields; the optimal temperature of our work was suggested to be 270 °C.

In addition, Figure 4b exhibits the effect of reaction time in lignin hydrogenolysis catalyzed by the $Ni_{12}P_5$/P−N−C−2 catalyst. The minimum value of phenolic monomer yield was 5.80% at 2 h, reached the maximum value of 9.60% at 4 h, and then decreased over time. The selectivity of alkylphenol was found to decrease with time. The content of alkylphenol reached the maximum at 2 h, accounted for 77.41% of the total monomer yield, and decreased to 73.61% at 8 h. This result indicated that the degree of esterification between oxidized lignin depolymerization products and ethanol in solvent increases with time. The yield of bio-oil reached the maximum (68.37%) at 2 h, and the yield of bio-oil decreased with the increase of reaction time. However, over 60% of the content of obtained bio-oil was retained. This indicates that the degree of repolymerization of dimers or oligomers increased with time, leading to a decrease in bio-oil and monomer yields.[42] Thus, the optimal reaction time was considered as 4 h.

In addition, the effect of catalyst dosage in lignin hydrogenolysis catalyzed by $Ni_{12}P_5$/P−N−C−2 was also investigated in detail. As shown in Figure 4c, the yield of bio-oil and the phenolic monomer was increased with raised catalyst dosage. The yield of bio-oil (38.16%) and the phenolic monomer (7.02%) was both the lowest at a lignin-to-catalyst mass ratio (L/C) of 0.2 g/0 g, and with the increase of catalyst input, both the yields reached the maximum value when L/C = 0.2 g/0.2 g. These results showed that the more the catalyst input, the more the $Ni^{\delta+}$ active sites for reaction, and the

https://doi.org/10.1021/acsomega.2c00564
ACS Omega 2022, 7, 13134−13143

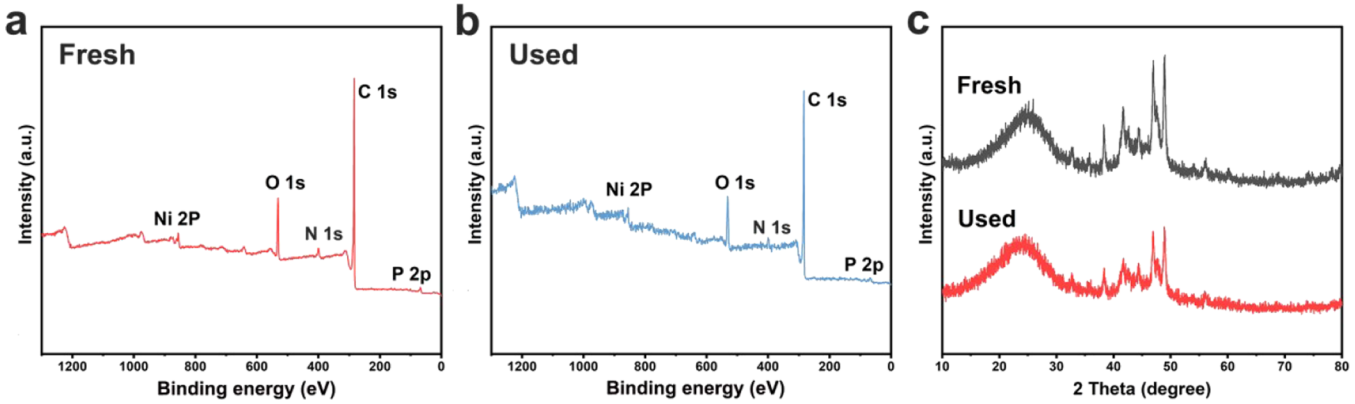

Figure 6. XPS survey curves of (a) fresh and (b) used $Ni_{12}P_5$/P−N−C−2 catalysts, and the (c) XRD pattern.

balance of the lignin catalytic hydrogenolysis reaction in the EtOH/iPrOH solvent was more toward the direction of generating oligomers and monomers and inhibiting the generation of char. The selectivity of alkylphenol was slightly decreased after the addition of the $Ni_{12}P_5$/P−N−C−2 catalyst, which dropped from 79.06% (noncatalytic run) to 76.15% (L/C = 0.2 g/0.2 g). This possibly indicated that the $Ni_{12}P_5$/P−N−C−2 catalyst has a certain degree of catalytic effect on the condensation reaction of the oxidized lignin depolymerization monomer with ethanol in the hydrogen-donating solvent.

3.4. Structural Changes in Aliphatic and Aromatic Regions of Lignin and Lignin-Based Bio-Oil. The 2D HSQC NMR spectra of noncatalyzed (Figure 5a,b) and catalyzed lignin (Figure 5c,d) exhibited the structure variation before and after catalysis. The proportion of syringl (S), guaiacyl (G), and *p*-hydroxyphenyl (H) subunits as well as the *β*-O-4 alkyl-aryl ethers (A, *β*-O-4) (47.98%), resinols (B, *β*-*β*) (2.24%), phenylcoumarans (C, *β*-5) (11.02%), spirodienones (D) (26.75%), and *α*, *β*-diaryl ethers (E) (12.01%) substructures was semiquantified by integrating the contour signals in Figure 6a based on the previous literature.[43] Previous research of del Río et al. had claimed that herbaceous plant lignin appeared to contain abundant p-coumarate.[44] Therefore, the plenty of p-coumarates (p-CE) and ferulates (p-FA) signals in aromatic regions of the HSQC spectra revealed that the feed lignin fractionated from herbaceous plants.[45] After hydrogenolysis reaction catalyzed by the $Ni_{12}P_5$/P−N−C−2 catalyst, the signals assigned to *β*-O-4 (A_α and A_β) totally disappeared, due to its low bond dissociation energy, which made *β*-O-4 linkage sensitive to the attack of the catalyst. Meanwhile, the intensity of p-coumarate and resinol (B_α and B_β) substructure signals was sharply decreased. The contours in the aromatic regions of bio-oil HSQC spectra were likely ascribed to the phenolic products obtained by lignin hydrogenolysis, and the methoxy group signals (δ_C/δ_H = 56.02/3.75) in aliphatic regions were ascribed to the existence of alkylphenol as shown in GC−MS data. The proportion of S/G/H in feed lignin was 39:34:27 (%) calculated using the HSQC spectrum, which turned to be 27:42:31 (%) after being catalyzed at 270 °C by the $Ni_{12}P_5$/P−N−C−2 catalyst. In addition, at 270 °C, the S/G/H ratio of lignin monomers was 19:50:31 (%) after catalysis and 20:51:29 (%) in the noncatalytic run. The content of G units in bio-oil as well as the proportion of G-type lignin monomer products catalyzed by the $Ni_{12}P_5$/P−N−C−2 catalyst was observed to increase in comparison with the noncatalytic run. Thus, the generation of G-type products should be one of the main reactions during the lignin conversion process. This result was also consistent with the distribution of monomer products determined by GC−MS and GC.

3.5. Changes of the $Ni_{12}P_5$/P−N−C Catalyst after Use. The structural change of the catalyst after use affected the reusability of the catalyst. Thus, the XPS survey analyses of fresh and 3 times used $Ni_{12}P_5$/P−N−C−2 catalysts were conducted as well as the XRD analysis. As shown in Figure 6a,b, the obvious signals of P 2p, C 1s, N 1s, O 1s, and Ni 2p existed in both fresh and used $Ni_{12}P_5$/P−N−C−2 catalysts. The distribution and binding energies of each element signal were similar. This proved that the valence state of the surface elements of the catalyst was the same before and after use, and the active sites of Ni, P, and N elements on the surface of the catalyst still possessed a high activity for the catalytic hydrogenolysis of lignin. The XRD curves of fresh and used $Ni_{12}P_5$/P−N−C−2 catalysts were also recorded as shown in Figure 6c. The existence of the intense $Ni_{12}P_5$ (312) peak at around 2θ = 48.92° was exhibited in the XRD patterns of both fresh and used $Ni_{12}P_5$/P−N−C−2 catalysts. The positions and intensities of diffraction peaks of other crystal planes also showed no significant difference in the two curves. These results indicated that the used $Ni_{12}P_5$/P−N−C−2 catalyst retained the catalytic reactivity well.

4. CONCLUSIONS

An $Ni_{12}P_5$/P−N−C catalyst was synthesized by a simple two-step method. Chlorella was used as a carbon source to support Ni^{2+} ions. Through one-step carbonization, $Ni_{12}P_5$ metal nanoparticles were uniformly dispersed on the catalyst surface. The catalyst obtained 65.26% bio-oil yield, 9.60% monomer yield, and 76.15% selectivity to alkylphenol in the product after reaction at 270 °C for 4 h in EtOH/iPrOH (1:1, v/v). In the mixed solvent, $Ni^{\delta+}$ active sites on the $Ni_{12}P_5$/P−N−C catalyst improved the hydrogen transfer capacity of the solvent and the yield of bio-oil and phenolic monomers compared with the reaction without the catalyst. Compared to the same types of catalysts that are already available, the use of high-risk and explosive H_2 was avoided in the lignin hydrogenolysis process, still resulting in relatively high product yields. The results recorded by 2D HSQC NMR and GC also confirmed that the $Ni_{12}P_5$/P−N−C catalyst possessed the ability to generate more G-type products. Due to the straightforward, cheap, safe process of the catalyst preparation and the lignin hydrogenolysis, this catalyst preparation method and lignin hydro-

https://doi.org/10.1021/acsomega.2c00564
ACS Omega 2022, 7, 13134−13143

genolysis pathway hold promising application prospects for the industrialization of lignin hydrogenolysis to prepare high-value phenolic compounds.

■ ASSOCIATED CONTENT

Supporting Information

The Supporting Information is available free of charge at https://pubs.acs.org/doi/10.1021/acsomega.2c00564.

High-magnification HR-TEM images of $Ni_{12}P_5$/C-8% catalysts; N_2 adsorption−desorption isotherms of DC, $Ni_{12}P_5$/P−N−C−1, $Ni_{12}P_5$/P−N−C−2, and $Ni_{12}P_5$/P−N−C−3 catalysts; pH value of $Ni(NO_3)_2$ aqueous solution with different concentrations at room temperature; possible bonding configurations of N atoms; relative content of each element in the three catalysts detected by SEM-EDS; BET surface area (SBET), pore volume, and pore diameter of catalysts; ICP-AES analysis for the $Ni_{12}P_5$/P−N−C catalysts (PDF)

■ AUTHOR INFORMATION

Corresponding Author

Xing Wang − *Liaoning Key Laboratory of Pulp and Paper Engineering, School of Light Industry and Chemical Engineering, Dalian Polytechnic University, Dalian 116034, PR China; Guangxi Key Laboratory of Clean Pulp & Papermaking and Pollution Control, College of Light Industry and Food Engineering, Guangxi University, Nanning 530004, PR China;* orcid.org/0000-0002-1539-5741; Email: wangxing@dlpu.edu.cn

Authors

Xin Zhao − *Liaoning Key Laboratory of Pulp and Paper Engineering, School of Light Industry and Chemical Engineering, Dalian Polytechnic University, Dalian 116034, PR China*

Yingying Yang − *Liaoning Key Laboratory of Pulp and Paper Engineering, School of Light Industry and Chemical Engineering, Dalian Polytechnic University, Dalian 116034, PR China*

Jingyu Xu − *Liaoning Key Laboratory of Pulp and Paper Engineering, School of Light Industry and Chemical Engineering, Dalian Polytechnic University, Dalian 116034, PR China;* orcid.org/0000-0002-6724-9623

Yanzhu Guo − *Liaoning Key Laboratory of Pulp and Paper Engineering, School of Light Industry and Chemical Engineering, Dalian Polytechnic University, Dalian 116034, PR China; Guangxi Key Laboratory of Clean Pulp & Papermaking and Pollution Control, College of Light Industry and Food Engineering, Guangxi University, Nanning 530004, PR China*

Jinghui Zhou − *Liaoning Key Laboratory of Pulp and Paper Engineering, School of Light Industry and Chemical Engineering, Dalian Polytechnic University, Dalian 116034, PR China*

Complete contact information is available at: https://pubs.acs.org/10.1021/acsomega.2c00564

Notes

The authors declare no competing financial interest.

■ ACKNOWLEDGMENTS

The authors acknowledge financial support from the National Natural Science Foundation of China (Nos. 21908014 and 22078035), the Special Financial Grant from the China Postdoctoral Science Foundation (No. 2020T130464) and the Foundation of Guangxi Key Laboratory of Clean Pulp & Papermaking and Pollution Control, College of Light Industry and Food Engineering, Guangxi University (No. 2021KF01).

■ REFERENCES

(1) Fatih Demirbas, M. Biorefineries for biofuel upgrading: A critical review. *Appl. Energy* **2009**, *86*, 151−161.

(2) Song, Q.; Wang, F.; Cai, J.; Wang, Y.; Zhang, J.; Yu, W.; Xu, J. Lignin depolymerization (LDP) in alcohol over nickel-based catalysts via a fragmentation−hydrogenolysis process. *Energy Environ. Sci.* **2013**, *6*, 994−1007.

(3) Fang, S.; Cui, Z.; Zhu, Y.; Wang, C.; Bai, J.; Zhang, X.; Xu, Y.; Liu, Q.; Chen, L.; Zhang, Q.; Ma, L. In situ synthesis of biomass-derived Ni/C catalyst by self-reduction for the hydrogenation of levulinic acid to γ-valerolactone. *J. Energy Chem.* **2019**, *37*, 204−214.

(4) Kim, J. Y.; Park, J.; Hwang, H.; Kim, J. K.; Song, I. K.; Choi, J. W. Catalytic depolymerization of lignin macromolecule to alkylated phenols over various metal catalysts in supercritical tert-butanol. *J. Anal. Appl. Pyrolysis* **2015**, *113*, 99−106.

(5) Chen, L.; Yu, Q.; Wang, Q.; Wang, W.; Qi, W.; Zhuang, X.; Wang, Z.; Yuan, Z. A novel deep eutectic solvent from lignin-derived acids for improving the enzymatic digestibility of herbal residues from cellulose. *Cellulose* **2019**, *26*, 1947−1959.

(6) Bjelić, A.; Grilc, M.; Likozar, B. Catalytic hydrogenation and hydrodeoxygenation of lignin-derived model compound eugenol over Ru/C: Intrinsic microkinetics and transport phenomena. *Chem. Eng. J.* **2018**, *333*, 240−259.

(7) Li, C.; Zhao, X.; Wang, A.; Huber, G. W.; Zhang, T. Catalytic Transformation of Lignin for the Production of Chemicals and Fuels. *Chem. Rev.* **2015**, *115*, 11559−11624.

(8) Leng, E.; Guo, Y.; Chen, J.; Liu, S.; E, J.; Xue, Y. A comprehensive review on lignin pyrolysis: Mechanism, modeling and the effects of inherent metals in biomass. *Fuel* **2022**, *309*, 122102−122136.

(9) Xu, J.; Li, M.; Qiu, J.; Zhang, X. F.; Yao, J. Photocatalytic depolymerization of organosolv lignin into valuable chemicals. *Int. J. Biol. Macromol.* **2021**, *180*, 403−410.

(10) Ma, R.; Guo, M.; Zhang, X. Recent advances in oxidative valorization of lignin. *Catal. Today* **2018**, *302*, 50−60.

(11) Huang, S.; Mahmood, N.; Tymchyshyn, M.; Yuan, Z.; Xu, C. Reductive de-polymerization of kraft lignin for chemicals and fuels using formic acid as an in-situ hydrogen source. *Bioresour. Technol.* **2014**, *171*, 95−102.

(12) Ye, K.; Liu, Y.; Wu, S.; Zhuang, J. A review for lignin valorization: Challenges and perspectives in catalytic hydrogenolysis. *Ind. Crops Prod.* **2021**, *172*, 114008−114018.

(13) Oregui-Bengoechea, M.; Gandarias, I.; Arias, P. L.; Barth, T. Solvent and catalyst effect in the formic acid aided lignin-to-liquids. *Bioresour. Technol.* **2018**, *270*, 529−536.

(14) Oregui-Bengoechea, M.; Gandarias, I.; Arias, P. L.; Barth, T. Unraveling the Role of Formic Acid and the Type of Solvent in the Catalytic Conversion of Lignin: A Holistic Approach. *ChemSusChem* **2017**, *10*, 754−766.

(15) Huang, N.; Yuan, S.; Drake, H.; Yang, X.; Pang, J.; Qin, J.; Li, J.; Zhang, Y.; Wang, Q.; Jiang, D.; Zhou, H.-C. Systematic Engineering of Single Substitution in Zirconium Metal−Organic Frameworks toward High-Performance Catalysis. *J. Am. Chem. Soc.* **2017**, *139*, 18590−18597.

(16) Tuci, G.; Liu, Y.; Rossin, A.; Guo, X.; Pham, C.; Giambastiani, G.; Pham-Huu, C. Porous Silicon Carbide (SiC): A Chance for Improving Catalysts or Just Another Active-Phase Carrier? *Chem. Rev.* **2021**, *121*, 10559−10665.

(17) Liang, Q.; Ye, L.; Huang, Z. H.; Xu, Q.; Bai, Y.; Kang, F.; Yang, Q. H. A honeycomb-like porous carbon derived from pomelo peel for use in high-performance supercapacitors. *Nanoscale* **2014**, *6*, 13831−13837.
(18) Zhang, F.; Li, G. D.; Chen, J. S. Effects of raw material texture and activation manner on surface area of porous carbons derived from biomass resources. *J. Colloid Interface Sci.* **2008**, *327*, 108−114.
(19) Hong, K. L.; Qie, L.; Zeng, R.; Yi, Z. Q.; Zhang, W.; Wang, D.; Yin, W.; Wu, C.; Fan, Q. J.; Zhang, W. X.; Huang, Y. H. Biomass derived hard carbon used as a high performance anode material for sodium ion batteries. *J. Mater. Chem. A* **2014**, *2*, 12733−12738.
(20) Plaza, M. G.; García, S.; Rubiera, F.; Pis, J. J.; Pevida, C. Evaluation of ammonia modified and conventionally activated biomass based carbons as CO2 adsorbents in postcombustion conditions. *Sep. Purif. Technol.* **2011**, *80*, 96−104.
(21) Tobimatsu, Y.; Chen, F.; Nakashima, J.; Escamilla-Trevino, L. L.; Jackson, L.; Dixon, R. A.; Ralph, J. Coexistence but independent biosynthesis of catechyl and guaiacyl/syringyl lignin polymers in seed coats. *Plant Cell* **2013**, *25*, 2587−2600.
(22) Scanlon, J. T.; Willis, D. E. Calculation of Flame Ionization Detector Relative Response Factors Using the Effective Carbon Number Concept. *J. Chromatogr. Sci.* **1985**, *23*, 333−340.
(23) Ramani, S.; Cogal, S.; Lowe, J.; Bhethanabotla, V. R.; Kuhn, J. N. Hybrid Co@Ni12P5/PPy microspheres with dual synergies for high performance oxygen evolution. *J. Catal.* **2020**, *391*, 357−365.
(24) Lan, X.; Hensen, E. J. M.; Weber, T. Hydrodeoxygenation of guaiacol over Ni2P/SiO2−reaction mechanism and catalyst deactivation. *Appl. Catal., A* **2018**, *550*, 57−66.
(25) Chen, B.; Rao, R.; Cao, M.; He, C.; Qian, Y.; Qiu, X.; Ouyang, X. Mild hydrodeoxygenation of lignin-derived bio-oils to hydrocarbons over bifunctional ZrP2O7-Ni12P5 catalysts. *Fuel* **2022**, *313*, 123044−123052.
(26) Yu, Z.; Wang, Y.; Liu, S.; Yao, Y.; Sun, Z.; Li, X.; Liu, Y.; Wang, W.; Wang, A.; Camaioni, D. M.; Lercher, J. A. Aqueous Phase Hydrodeoxygenation of Phenol over Ni3P-CePO4 Catalysts. *Ind. Eng. Chem. Res.* **2018**, *57*, 10216−10225.
(27) Li, T.; Lin, H.; Ouyang, X.; Qiu, X.; Wan, Z. In Situ Preparation of Ru@N-Doped Carbon Catalyst for the Hydrogenolysis of Lignin To Produce Aromatic Monomers. *ACS Catal.* **2019**, *9*, 5828−5836.
(28) Ren, J.; Cao, J. P.; Zhao, X. Y.; Wei, F.; Liu, T.-L.; Fan, X.; Zhao, Y. P.; Wei, X. Y. Preparation of high-dispersion Ni/C catalyst using modified lignite as carbon precursor for catalytic reforming of biomass volatiles. *Fuel* **2017**, *202*, 345−351.
(29) Northcote, D. H.; Goulding, K. J.; Horne, R. W. The Chemical Composition and Structure of the Cell Wall of Chlorella pyrenoidosa. *Biochem. J.* **1958**, *70*, 391−397.
(30) Safi, C.; Zebib, B.; Merah, O.; Pontalier, P. Y.; Vaca-Garcia, C. Morphology, composition, production, processing and applications of Chlorella vulgaris: A review. *Renew. Sustainable Energy Rev.* **2014**, *35*, 265−278.
(31) Wehrheimlj, B.; Wetter, M. Comparative studies of the heavy metal uptake of whole cells and different types of cell walls from chlorella fusca. *Biotechnol. Tech.* **1994**, *8*, 227−232.
(32) El-Sheekh, M. M.; El-Naggar, A. H.; Osman, M. E. H.; El-Mazaly, E. Effect of cobalt on growth, pigments and the photosynthetic electron transport in Monoraphidium minutum and Nitzchia perminuta. *Braz. J. Plant Physiol.* **2003**, *15*, 159−166.
(33) Yee, N.; Benning, L. G.; Phoenix, V. R.; Ferris, F. G. Characterization of Metal-Cyanobacteria Sorption Reactions: A Combined Macroscopic and Infrared Spectroscopic Investigation. *Environ. Sci. Technol.* **2004**, *38*, 775−782.
(34) Benning, L. G.; Phoenix, V. R.; Yee, N.; Tobin, M. Molecular characterization of cyanobacterial silicification using synchrotron infrared micro-spectroscopy. *Geochim. Cosmochim. Acta* **2003**, *68*, 729−741.
(35) Cheng, C.; Truong, J.; Barrett, J. A.; Shen, D.; Abu-Omar, M. M.; Ford, P. C. Hydrogenolysis of Organosolv Lignin in Ethanol/Isopropanol Media without Added Transition-Metal Catalyst. *ACS Sustainable Chem. Eng.* **2019**, *8*, 1023−1030.
(36) Kim, J. Y.; Park, J.; Kim, U. J.; Choi, J. W. Conversion of lignin to phenol-rich oil fraction under supercritical alcohols in the presence of metal catalysts. *Energy Fuels* **2015**, *29*, 5154−5163.
(37) Huang, X.; Koranyi, T. I.; Boot, M. D.; Hensen, E. J. Catalytic depolymerization of lignin in supercritical ethanol. *ChemSusChem* **2014**, *7*, 2276−2288.
(38) Wang, X.; Rinaldi, R. Solvent effects on the hydrogenolysis of diphenyl ether with Raney nickel and their implications for the conversion of lignin. *ChemSusChem* **2012**, *5*, 1−1466.
(39) Cheng, C.; Li, P.; Yu, W.; Shen, D.; Jiang, X.; Gu, S. Nonprecious Metal/Bimetallic Catalytic Hydrogenolysis of Lignin in a Mixed-Solvent System. *ACS Sustainable Chem. Eng.* **2020**, *8*, 16217−16228.
(40) Huang, X.; Atay, C.; Korányi, T. S. I.; Boot, M. D.; Hensen, E. J. M. Role of Cu-Mg-Al Mixed Oxide Catalysts in Lignin Depolymerization in Supercritical Ethanol. *ACS Catal.* **2015**, *5*, 7359−7370.
(41) Zhang, C.; Li, H.; Lu, J.; Zhang, X.; MacArthur, K. E.; Heggen, M.; Wang, F. Promoting Lignin Depolymerization and Restraining the Condensation via an Oxidation−Hydrogenation Strategy. *ACS Catal.* **2017**, *7*, 3419−3429.
(42) Lahive, C. W.; Deuss, P. J.; Lancefield, C. S.; Sun, Z.; Cordes, D. B.; Young, C. M.; Tran, F.; Slawin, A. M.; de Vries, J. G.; Kamer, P. C.; Westwood, N. J.; Barta, K. Advanced Model Compounds for Understanding Acid-Catalyzed Lignin Depolymerization: Identification of Renewable Aromatics and a Lignin-Derived Solvent. *J. Am. Chem. Soc.* **2016**, *138*, 8900−8911.
(43) Wen, J. L.; Yuan, T. Q.; Sun, S. L.; Xu, F.; Sun, R. C. Understanding the chemical transformations of lignin during ionic liquid pretreatment. *Green Chem.* **2014**, *16*, 181−190.
(44) del Río, J. C.; Lino, A. G.; Colodette, J. L.; Lima, C. F.; Gutiérrez, A.; Martínez, Á. T.; Lu, F.; Ralph, J.; Rencoret, J. Differences in the chemical structure of the lignins from sugarcane bagasse and straw. *Biomass Bioenergy* **2015**, *81*, 322−338.
(45) Xiao, L. P.; Wang, S.; Li, H.; Li, Z.; Shi, Z. J.; Xiao, L.; Sun, R. C.; Fang, Y.; Song, G. Catalytic Hydrogenolysis of Lignins into Phenolic Compounds over Carbon Nanotube Supported Molybdenum Oxide. *ACS Catal.* **2017**, *7*, 7535−7542.

https://doi.org/10.1021/acsomega.2c00564
ACS Omega 2022, 7, 13134−13143